Thermally Induced Proliferation of Pores in a Model Fluid Membrane

Julian C. Shillcock and Udo Seifert
Max-Planck-Institut für Kolloid- und Grenzflächenforschung, 14513 Teltow-Seehof, Germany

ABSTRACT The growth of thermally induced pores in a two-dimensional model fluid membrane is investigated by Monte Carlo simulation. Holes appear in the membrane via an activated process, and their subsequent growth is controlled by an edge energy per unit length or line tension. The barrier height and line tension, together with a lateral tension, are the independent parameters of the model. In the resulting phase diagram, a rupture transition separates an intact membrane from a disintegrated state. The approach to the ruptured state shows distinct regimes. Reducing the barrier height at large line tension produces multiple, quasi-independent, small holes whose behavior is dominated by their edge energy, whereas at lower line tensions shape fluctuations of the holes facilitate their coalescence into a single large hole. At a small value of line tension and large barrier height, a single hole spontaneously permeabilizes the membrane in an entropically driven phase transition. Entropy dominates pore growth for line tensions not far below those measured for artificial vesicles. Permeabilization of lipid bilayers by certain peptides involves perturbing lipid-lipid cohesive energies, and our simulations show that at small line tensions the entropy of hole shape fluctuations destroys the model membrane's stability.

INTRODUCTION

The viability of a cell depends on maintaining an intact plasma membrane that prevents the uncontrolled passage of material through it. The fluid lipid bilayer surrounding cells provides such an insulating barrier as a result of the hydrophobic effect. Cellular processes depend on the controlled transport of material across the membrane, whereas the artifical vesicles used in drug delivery systems must be resistant to stress induced by lytic agents in the host. A better understanding of the behavior of pores in fluid membranes is crucial to understanding the processes of material transport across cell membranes, pore formation by adsorbed peptides, and the mechanisms used by cells to anneal structural defects from the plasma membrane.

Many experiments on pore formation avoid the complexity of biological membranes (Sackmann, 1995) by using one-component lipid bilayers, either artificial vesicles or black lipid membranes (BLMs). Electroporation experiments show that BLMs rupture irreversibly when subjected to a transient electric field of $\sim$1 V that lasts for at least several microseconds (Abidor et al., 1979; Needham and Hochmuth, 1989; Wilhelm et al., 1993; Winterhalter, 1996). In contrast, micropipette experiments on vesicles have shown that pores may be held open in a quasistationary state for several seconds before resealing (Zhelev and Needham, 1993). This surprising result has been explained in terms of a dynamic stabilization of the pore arising from the friction experienced by the aspirated portion of the vesicle as it moves further into the pipette (Moroz and Nelson, 1997).

Received for publication 22 September 1997 and in final form 12 January 1998.

Address reprint requests to Dr. Udo Seifert, Max-Planck-Institut für Kolloid- und Grenzflächenforschung, Kantstrasse 55, 14513 Teltow-Seehof, Germany. Tel.: 49-3328-46594; Fax: 49-3328-46212; E-mail: useifert@mpikg-teltow.mpg.de.

0006-3495/98/04/1754/13 $2.00

A membrane subject to an electric field experiences an electrocompressive stress, causing it to thin (Crowley, 1973; Needham and Hochmuth, 1989). Thermally generated transient defects, in which lipid headgroups fluctuate apart, exposing their hydrocarbon tails to the aqueous medium, are thereby encouraged. The energy cost of such defects, referred to as hydrophobic pores, is essentially the energy of the exposed hydrocarbon-water interface (Helfrich, 1974). It is energetically favorable for the lipids around a large hydrophobic pore to reorient, overcoming an energy barrier so that their headgroups point into the pore channel, and form a hydrophilic pore (Glaser et al., 1988). The conductance of hydrophilic pores during reversible electroporation has been followed by various techniques: charge collapse across an initially charged membrane (Glaser et al., 1988), the fluorescence of voltage-sensitive dyes (Hibino et al., 1993), and directly in video microscopy (Zhelev and Needham, 1993). A recent set of experiments (Neumann and Kakorin, 1996) has used a fluorescent dye, whose absorption of polarized light varies with its orientation, to follow the degree of lipid reorientation during the time course of electroporation. Additional experiments on vesicles have included osmotic pressure-induced pore formation (Taupin et al., 1975) and the effect of vesicle polydispersity on interpreting the leakage of self-quenching dyes from artifical vesicles under osmotic stress (Hallett et al., 1993).

Most theories of pore formation to date derive from a simple model suggested more than 20 years ago by Litster (1975) and developed extensively by other groups (Abidor et al., 1979; Barnett and Weaver, 1991; Freeman et al., 1994). This model proposes that the appearance of a circular pore, of radius r, in a membrane under lateral tension Γ is associated with a reduction in energy $\pi r^2\Gamma$, and opposed by an edge energy proportional to the pore perimeter $2\pi r\Lambda$. The net energy change is thus $E(r) = 2\pi r\Lambda - \pi r^2\Gamma$. The line tension Λ derives from the hydrophobic property of the lipid molecules (Helfrich, 1974; Tanford, 1991) and creates

a barrier against pore formation, which is reduced by the surface tension Γ and, in electroporation experiments, an electric field-induced stress. A pore with a radius larger than the critical value Λ/Γ is predicted to grow without bound, and a membrane is only metastable against such pores when the critical energy barrier $\pi\Lambda^2/\Gamma$ is accessible to thermal fluctuations. Experiments have shown that typical values of the line tension are in the range $1–3 \times 10^{-11}$ N (Zhelev and Needham, 1993), and so the edge energy of a 1-nm-radius pore is on the order of $15–45k_BT$ at room temperature. A model of electroporation incorporating features elucidated over many years has been published recently (Freeman et al., 1994, and references therein). In this model, small, circular pores created via an Arrhenius process evolve according to a Smoluchowski equation in pore radius space. Like experimental results, the model predicts that pores that grow beyond a critical size rupture the membrane, whereas many small pores collapse the electric field on the membrane, allowing it to reseal.

Alternative models for the appearance of pores in a fluid lipid bilayer have been proposed. Spontaneous fluctuations in the bilayer thickness were suggested by Popescu et al. (1991), although they calculated an energy barrier of $91k_BT$ against such pores, suggesting that they are highly unlikely in unperturbed membranes. A lattice model in which the constituent lipids make transitions among a discrete number of orientational states in response to an applied electric field was suggested by Sugar and Neumann (1984). In another lattice model, Kaschiev and Exerowa (1983) proposed that thermally generated lipid defects (i.e., vacancies) aggregate and, if the chemical potential of the membrane lipids is sufficiently low, undergo a first-order van der Waals-like transition to a condensed phase of defects (i.e., a pore). Recent lattice Monte Carlo simulations of diblock copolymers dissolved in bulk homopolymer (Müller and Schick, 1996) have demonstrated that polydisperse pores form in a model bilayer when the chemical potential is below the critical micelle concentration. A field-theoretic model of pore formation in lamellar stacks of membranes subject to a stretching tension has been solved within mean field theory (Netz and Schick, 1996). This model predicts that pores already form when the membrane area is increased by just 2%, as found in experiments, and that they can form a condensed phase in the bilayer.

The structural integrity of lipid bilayers is also compromised by the absorption of foreign molecules. Peptides such as alamethicin, which lyses bacterial membranes (He et al., 1996; Wu et al., 1995); melittin, a bee venom (Matsuzaki et al., 1997b); and magainin (Ludtke et al., 1996) induce leakage in lipid bilayers, the magnitude of the effect depending on the peptide concentration (Dimitrova and Matsumura, 1997; Heller et al., 1997; Ludtke et al., 1996; Matsuzaki et al., 1997a). Magainin makes a transition from being mainly adsorbed on the surface to projecting transversely across the bilayer as the concentration is increased. Unlike alamethicin, which lines the perimeter of the pores it creates, leading to a so-called barrel-stave pore (He et al., 1996; Huang and Wu, 1991), only three or four magainin molecules are required to stabilize a pore. Both electrostatic and hydrophobic interactions play a role in peptide-membrane interactions (Matsuzaki et al., 1997a; Beschiaschvili and Seelig, 1991). The orientation of peptides, and their effects on the lipid headgroup position, have been investigated by circular diochroism (Heller et al., 1997), and peptides have been found to diffuse freely within the membrane plane, allowing pores to be formed at random locations (Beschiaschvili and Seelig, 1991). Experiments that incorporate hydrocarbons or steroid derivatives into cell membranes have shown that they perturb the natural membrane fluidity and cohesion near the main transition (Ghosh et al., 1996; Sabra et al., 1996). Furthermore, cholesterol increases the resistance of stearoyloleoylphosphatidylcholine (SOPC) vesicles to pore formation (Needham and Hochmuth, 1989; Zhelev and Needham, 1993). The passive permeability of vesicles near the main transition is also altered by the incorporation of foreign molecules into the vesicle membrane (cardiolipid in Shibata et al., 1994; cholesterol in Parasassi et al., 1995; ethanol in Komatsu and Okada, 1996; corticosteroids in Ghosh et al., 1996; and lindane in Sabra et al., 1996). Cholesterol has been proposed to create irregular, heterogeneous domains within the lipid bilayer that allow increased transport of molecules across the membrane (Parasassi et al., 1995). The energy of such domains is typically proportional to their perimeter. The addition of edge-active agents to lipid bilayers can greatly reduce the edge energy of pores and promote their growth (Fromherz, 1983). Although the pores formed by alamethicin and magainin are only a few nanometers in diameter, and involve perhaps a dozen or so lipids, membrane lysis involves the growth of pores to much larger sizes and destabilization of the membrane. The free energy of such holes includes an entropic contribution from edge shape fluctuations that cannot be modeled by energy-dominated, circular pores.

In this work we use Monte Carlo simulations to investigate the behavior of multiple holes in a model fluid membrane. Hydrophilic pores in lipid bilayers are thought to result from the growth of hydrophobic defects with a linear scale less than a lipid headgroup diameter (Glaser et al., 1988). Because the energetics of this molecular reorientation is unknown, we model hole growth by two steps: thermal fluctuations overcome an energy barrier to create minimal-sized holes (corresponding to the subnanometer hydrophilic pores of Glaser et al., 1988); and subsequent evolution of the holes is controlled by a constant line tension. Such a distinction is reasonable for membranes under lateral tension (BLMs in electroporation) and in the absence of tension (pore-forming peptides adsorbing onto lipid bilayers). The parameters of our model are the barrier height against hole creation, the line tension, and a lateral (stretching) tension. The electric field in electroporation is represented by modulating the energy barrier, and the effect of membrane components (such as cholesterol) that alter the lipid bilayer's cohesive properties is contained in the line

tension. Our model is also relevant to experiments that use peptides to create pores in lipid bilayers. In this case, increasing the amount of peptide adsorbed on the membrane surface is represented by reducing the barrier height against hole formation, and the action of the peptide in perturbing the lipid cohesion or packing around a pore is modeled by the line tension.

Our simulations show that the hole shape fluctuations and interactions lead to a more complicated phase diagram than is explicable by assuming circular pores. Previous Monte Carlo simulations of a single hole in a model fluid membrane (Shillcock and Boal, 1996) appear here as the boundary to the intact membrane state for large hole creation barrier heights. A closed-to-open transition was also found in a three-dimensional simulation of a fluid membrane patch driven by the competition between the edge energy around the membrane and its bending energy (Boal and Rao, 1992). The line tension required to convert the open membrane patch with zero rigidity into a closed vesicle is 25% less than the critical line tension for closure of a hole in our two-dimensional membrane. The hole shape fluctuations are not destroyed when the network is subject to a stretching tension, and the approach to rupture is different for networks at small and large line tensions. Our model phase diagram shows that entropy can undermine the stability of a dynamic system, such as a lipid bilayer, and render zero-temperature calculations inapplicable.

The paper is organized as follows. We first briefly describe the Monte Carlo simulations of multiple holes. Next we present the results of the simulations and compare them with simple analytic calculations. Details of model calculations are given in Appendix A, and a description of the Monte Carlo algorithm is relegated to Appendix B.

MONTE CARLO SIMULATION METHOD

Our fluid membrane model is derived from that introduced a decade ago by Kantor et al. (1986). The membrane is represented by a triangulated network of N_v vertices connected by $3N_v$ straight, flexible edges or bonds occupying a rectangular patch with side lengths L_x, L_y embedded in two-dimensional space. The number of vertices in the network is constant, whereas the number of bonds varies as holes appear and disappear. The network is rendered fluid by allowing vertices to break and reconnect the bonds between them in a move proposed by Baumgartner and Ho (1990). A vertex can have between 3 and 12 connected neighbors, the lower limit ensuring that the network remains simply connected. The vertices, hard disks of diameter a, set the length scale in the simulations. All pairs of vertices are prevented from approaching closer than a distance a, and the energy of the bonds between nearest-neighbor vertices is zero unless the bond is stretched beyond a maximum length, $1.688a$ (chosen to prevent bond crossing) or reduced below a, when the energy is infinite. Thus the network possesses only entropic elasticity. A configuration of a network specifies the coordinates of all of the vertices, the connectivity of the bonds, and the labeling of those vertices on the boundaries of holes. A maximum of 100 holes is allowed, but this constraint is never reached. Vertices defining the edge of a hole are called external, and may be on the boundary of at most one hole, whereas vertices in the interior of a network are internal. Typical configurations of networks with several holes are shown in the shapshots of Fig. 1.

A hole is created in the computational membrane by the removal of a single internal bond, creating a minimal-sized hole that has four external bonds on its boundary. The energy cost associated with creating such a hole is Q, and represents the barrier height that thermal fluctuations must overcome to create a minimal-sized hydrophilic pore in a lipid bilayer. A constant line tension, Λ, represents the energy cost per unit length for lipids to move from the bulk membrane onto the pore perimeter, and hole growth occurs in the computational network by the removal of external bonds from the edge of a hole. The energy cost associated with hole growth is equal to the product of the line tension and the change in hole perimeter length. Holes shrink by adding bonds back along their boundaries, and the disappearance of a hole takes place when a bond is added across

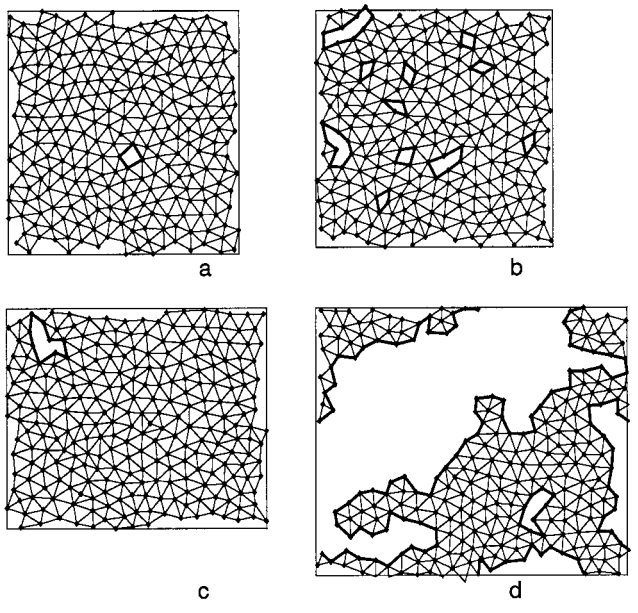

FIGURE 1 Snapshots of a 256-vertex fluid network along two paths in the reduced line tension-reduced barrier height (λ,q) phase diagram of Fig. 2. Hole edge bonds are shown thicker than internal bonds. A membrane with $\lambda = 4$ and $q = 9.3$ and $q = 4.3$ is shown in configurations a and b, respectively. The number of small holes increases at smaller q, but they remain almost independent for the barrier heights shown. The lower configurations (c and d) show a membrane with $\lambda = 1.25$ and $q = 10.2$ and $q = 8.2$, respectively. In this regime, there are only one or two small holes at large q, and a single hole grows to occupy the membrane as q is reduced. The membrane is periodic in both directions (and simply connected), but the bonds that cross the simulation box boundaries have not been drawn for clarity. The side lengths of the simulation box are drawn to scale, but the vertices (whose diameter sets the length scale in the simulation) are reduced in size for clarity. The membrane area is approximately constant, but the simulation box area increases as holes grow.

a hole with four external vertices. The moves to simulate hole behavior satisfy detailed balance and are described in Appendix B. A lateral tension, P, is introduced that couples to the area of the simulation box.

Model parameters are expressed in dimensionless combinations. The reduced line tension and barrier height against hole creation are

$$\lambda = \beta\Lambda a \quad \text{and} \quad q = \beta Q, \tag{1}$$

where a is the unit of length in the simulations and $\beta = 1/k_BT$, with temperature T and Boltzmann's constant k_B. Mechanical stability requires that the line tension and barrier height be positive. The reduced lateral tension on the membrane is

$$p = \beta P a^2. \tag{2}$$

Lowercase variable names represent reduced quantities in the remainder of the paper. The absence of a bond potential energy function means that the temperature appears only as a prefactor to these parameters.

A simulation begins with the vertices placed at the lattice points of a regular triangular lattice, and no holes are present in the network. Rectangular periodic boundary conditions are used to minimize the effects of the system size. The network evolves by applying the Metropolis algorithm to translate all of the vertices; introduce holes; allow them to grow, shrink, coalesce, or fragment and disappear; and simulate the network fluidity and area fluctuations. We check that successive configurations are independent by measuring the serial correlation times for observables of interest (e.g., hole perimeter, hole area, and membrane area) and setting the number of discarded sweeps greater than the relevant correlation time. Configurations are separated by at least $N_v/\Delta s^2$ sweeps (typically 50,000–100,000), where Δs is the maximum step size for vertex translations, and the initial ordered state of the network is allowed to equilibrate by discarding 100 times this many sweeps before configurations are stored for analysis. The ensemble average of an observable is denoted by angle brackets; 1000 configurations are used to calculate such averages. Observables that take distinct values for each hole, such as its area or perimeter, are first averaged over all of the holes within each configuration before constructing the ensemble averages. In cases where the fluctuations of an observable are large, up to five independent simulations are used to provide ensemble averages.

RESULTS

We have used Monte Carlo simulations to investigate the stability of a model fluid membrane to multiple hole formation from a regime in which no holes are created within the duration of a simulation, to one in which the membrane is intrinsically unstable to disintegration. Most of the results presented are for membranes under zero lateral tension for which the network area fluctuates about an average size determined by its entropic elasticity, although we also comment briefly on the results for membranes under tension.

Phase diagram with rupture transition

A phase diagram of the membrane state as a function of the reduced line tension λ and hole creation barrier height q at zero lateral tension is shown in Fig. 2. The membrane exhibits two distinct equilibrium regimes: intact and ruptured. The two regimes are separated by a phase boundary, the rupture transition (shown as the *thick line* in Fig. 2), which may be characterized as a function of the reduced barrier height or, equivalently, the line tension:

$$\lambda = \lambda_R(q) \quad \text{or} \quad q = q_R(\lambda). \tag{3}$$

The asymptotes marking the boundaries of the ruptured state occur at

$$\lambda^* \equiv \lambda_R(q \to \infty) = 1.24 \pm 0.02$$

and (4)

$$q^* \equiv q_R(\lambda \to \infty) = 3.3 \pm 0.2.$$

The computational definition of the ruptured state at zero lateral tension is given in the next subsection. Holes appear

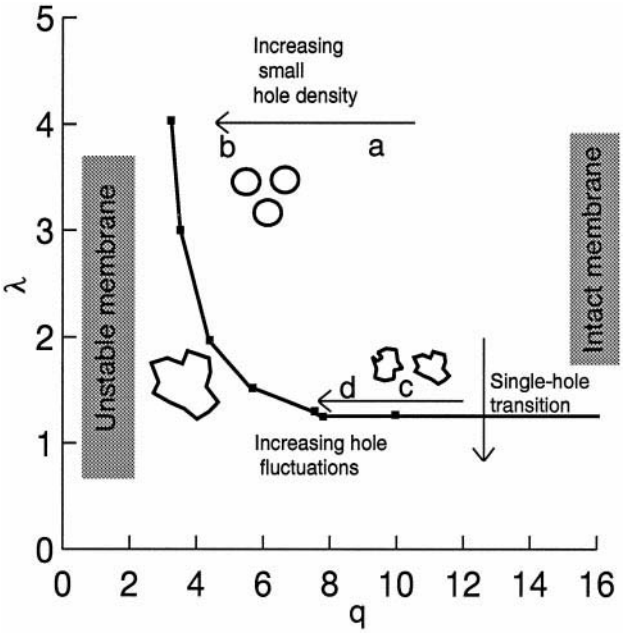

FIGURE 2 Phase diagram of model fluid membrane in the reduced line tension-reduced barrier height (λ,q) plane at zero stretching tension. The bold line denotes the rupture transition separating an intact membrane from a disintegrated one, and the symbols mark simulation data. At large line tensions, multiple small holes are present in the membrane, and a single, large hole fluctuates through the membrane for λ close to 1.25. The upper horizontal arrow represents a possible path for rupture at large λ in which more small holes are created as q is reduced, and corresponds to snapshots *a* and *b* in Fig. 1; the lower horizontal arrow represents rupture at small λ and is illustrated in snapshots *c* and *d* of Fig. 1. Rupture via the entropy-driven growth of a single fluctuating hole is indicated by the vertical arrow.

in the membrane within the intact regime as q is lowered. When the reduced line tension λ is large, an increasing number of small holes appear as q is reduced, whereas for $\lambda \gtrsim \lambda^*$, only a few holes appear, and one of them fluctuates greatly and increases in size as q is reduced. When $q < q_R(\lambda)$, the computational membrane is intrinsically unstable as the holes occupy most of the simulation box.

Two possible paths for a membrane at fixed line tension subject to an increasing probability of hole creation are shown by horizontal arrows in Fig. 2. The upper arrow represents a membrane with a line tension $\lambda = 4$. The membrane is initially intact at large q; with no holes present, it passes through a regime of increasing number of small holes as q is reduced, and finally enters the unstable regime at $\lambda_R(4) \simeq 3.3$. Snapshots of typical membrane configurations at $q = 9.3, 4.3$ are shown in *a* and *b* of Fig. 1. Along this path, the regime of increasing hole number is well described by a model that treats the holes as an ideal gas in two dimensions (see Discussion). A different scenario applies to the lower horizontal arrow, illustrating a membrane with line tension $\lambda = 1.25$, just above the limiting value λ^*. There are one or two small holes in the membrane at large q, but now reducing the barrier height causes one hole to grow and fluctuate throughout the membrane. The average size and shape fluctuations of the dominant hole increase as q is reduced until the unstable regime is entered. Configurations of the membrane at $q = 10.2, 8.2$ are illustrated in *c* and *d* of Fig. 1. The convoluted shape of the large hole is evident.

The vertical arrow in Fig. 2 indicates a path through the rupture transition at large q, along which the membrane passes from the intact state with no holes to a ruptured state with a single large, fluctuating hole as the line tension is reduced through $\lambda_R(q)$ of Eq. 4. When $\lambda < \lambda_R(q)$, the growth of the hole is driven irreversibly by the entropy of its shape fluctuations, and the equilibrium membrane state is disintegrated. This transition was found in previous simulations of a single hole in a fluid network (Shillcock and Boal, 1996). It reappears here as the boundary of the disintegrated state in the limit $q \to \infty$, where the large barrier height makes the appearance of more than a single hole very unlikely. The reader is referred to the earlier work for a theory of this transition. Concerning the character of the transition of the stable membrane to the ruptured state, the bimodal distribution of hole sizes discussed below suggests it is first order. However, the approach of the membrane toward the ruptured state proceeds by qualitatively distinct mechanisms for large and small line tension.

In the following subsections we present the data on which the phase diagram is based, and discuss their system size dependence.

Number and size of holes

When the hole creation barrier height is inaccessible to thermal fluctuations on the time scale of a simulation, the network is intact and behaves as a typical fluid membrane, in agreement with previous simulations (Shillcock and Boal, 1996; Boal et al., 1992). Holes are introduced into the network as the energy barrier q is reduced. The logarithm of the average number of holes in a 256-vertex network, $\ln\langle N\rangle$, is plotted against the dimensionless barrier height q in Fig. 3 for line tensions λ 1.2, 1.25, 1.3, 1.5, 2.0, 4.0. Some data at other line tensions are omitted for clarity. The number of holes in networks with line tensions $\lambda \leq 1.3$ show little systematic variation with q and are independent of the system size. Typical data for $\lambda = 1.25$ and $q = 10.2, 8.2$, respectively, are $\langle N\rangle = 1.02 \pm 0.12, 1.06 \pm 0.23, 1.05 \pm 0.21, 1.10 \pm 0.30$, and $\langle N\rangle = 1.20 \pm 0.44, 1.34 \pm 0.62, 1.40 \pm 0.67, 1.36 \pm 0.65$ for system sizes $N_v = 144, 196, 256, 400$. Visual inspection of the configurations shows that there is a single hole that dominates the membrane, with occasionally one or two smaller ones coexisting with it. Networks with $\lambda \leq 1.3$ move from a regime in which the average hole perimeter is small and independent of N_v at large q to one in which the hole perimeter length and its fluctuations are proportional to N_v as q approaches $q_R(\lambda)$ (data not shown).

Networks with $\lambda \geq 1.5$ possess a regime in which the number of holes grows exponentially over a range of q that increases with increasing line tension. In this regime, the number of holes in the network may increase by an order of magnitude before the system size limitation is reached. The number of holes per vertex for a network with $\lambda = 4$ and $q = 6.3$ (midway between snapshots *a* and *b* in Fig. 1) and $q = 4.3$ are, respectively, $\langle N\rangle/N_v = 0.016, 0.016, 0.016, 0.015$, and $\langle N\rangle/N_v = 0.057, 0.059, 0.059, 0.059$ for system sizes $N_v = 144, 196, 256, 400$, respectively. The number of

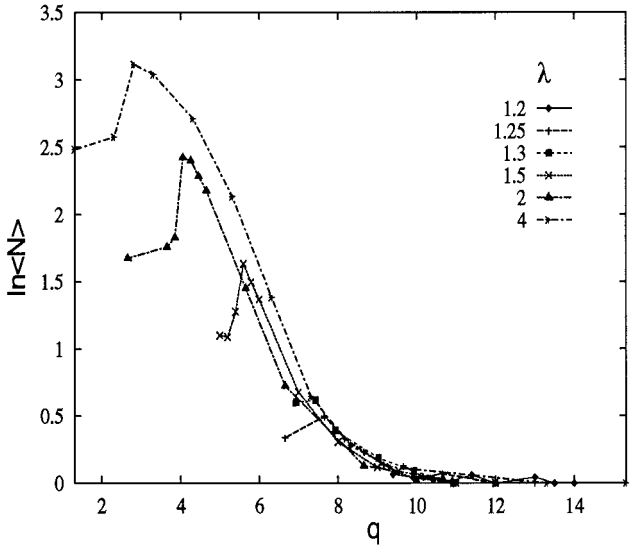

FIGURE 3 Logarithm of the average number of holes $ln\langle N\rangle$ in a 256-vertex network as a function of the reduced barrier height q for reduced line tensions $\lambda = 1.2, 1.25, 1.3, 1.5, 2.0, 4.0$. Networks with $\lambda < 1.5$ show no systematic increase in hole density as q is lowered. When $\lambda \geq 1.5$, there is an exponential increase in hole density as described in the text. The downturn in the curves at small q results from the finite system size.

holes is directly proportional to the system size N_v, even for q close to the rupture transition $q_R(\lambda)$, suggesting that the holes are independent. The total hole perimeter length and area are also proportional to N_v, so that the average hole area and perimeter length are independent of the system size (data not shown). The number of holes remains proportional to N_v for line tensions down to $\lambda = 1.5$ for $q \gg q_R(\lambda)$, but starts to become sublinear, indicating hole coalescence, for $q \gtrsim q_R(\lambda)$.

The membrane enters the unstable regime when the aggregate hole area approaches that of the simulation box. The number of holes decreases at the extreme left of the curves in Fig. 3 as a result of the finite system size, forcing holes to coalesce. The rupture boundary separating the intact and unstable regimes in the phase diagram (Fig. 2) is computationally defined as the values of λ,q from the last simulation before the system size limit is reached in a sequence of runs at fixed λ and decreasing q. For line tensions $\lambda > 2$, there is negligible change in quantities such as the compression modulus, average hole perimeter, and area for system sizes between 144 and 400 vertices. Networks with line tensions in the range $1.25 < \lambda < 2$ show a variation in the location of the boundary that is less than ± 0.2 in q for system sizes 144 to 400 vertices.

The dimensionless average hole perimeter multiplied by the line tension $\lambda\langle L_{ave}\rangle/a$ is shown in Fig. 4 as a function of q. The average is calculated over the set of holes in each configuration before performing the ensemble average. Networks with line tensions $\lambda = 4$, 2, 1.5 have a regime in which $\lambda\langle L_{ave}\rangle/a$ is independent of q over a range that increases with increasing λ. This corresponds to the period of exponential growth in hole number seen in Fig. 3. The predictions of the ideal pore gas model (Eq. 12 in Appendix A) for $\lambda\langle L_{ave}\rangle/a$ are shown by arrows for the two cases $\lambda = 4$, 2, and the agreement is very good. Data at $\lambda = 3$ also satisfying the equation have been omitted for clarity. When the line tension is $\lambda < 1.5$, the average hole perimeter increases to a large value as q is reduced without passing through a q-independent region. At a line tension $\lambda = 1.2$, the average hole perimeter first decreases with increasing q, but then shows large excursions for $q = 12$ to $q = 14$. Examination of snapshots of these networks shows that a large hole sometimes briefly appears during the simulations before resealing. As described in the previous section, networks with small λ are only metastable to the appearance of a hole whose catastrophic growth is driven by the entropy of its shape fluctuations. Such a hole would always rupture the network in an infinitely long simulation, but may be suppressed by the exponential dependence of the hole creation rate on q in a finite simulation. Furthermore, the finite network size allows a large hole to shrink and disappear, reappearing later in the simulation. Such effects complicate the extraction of the "average" hole size from a finite simulation. Inspection of the time series of the hole area for the case $\lambda = 1.2$, $q = 13$ shows that a single hole appeared for only 2.3% of the total simulation time, but had 100 vertices around its perimeter and a maximum area of $A/a^2 = 285$ compared to an average membrane area for this simulation of $A_{mem}/a^2 = 378 \pm 13$ (data not shown). Independent simulations at constant λ,q showed such excursions once or twice in 1000 configurations, and given that they can occur repeatedly in longer simulations, we conclude that the intact membrane is only metastable at $\lambda = 1.2$. This behavior was never seen for $\lambda \geq 1.25$, despite repeated simulations. The network was never intact for $\lambda = 1.1$ and barrier heights in the range $q = 12.5$–14 (data not shown).

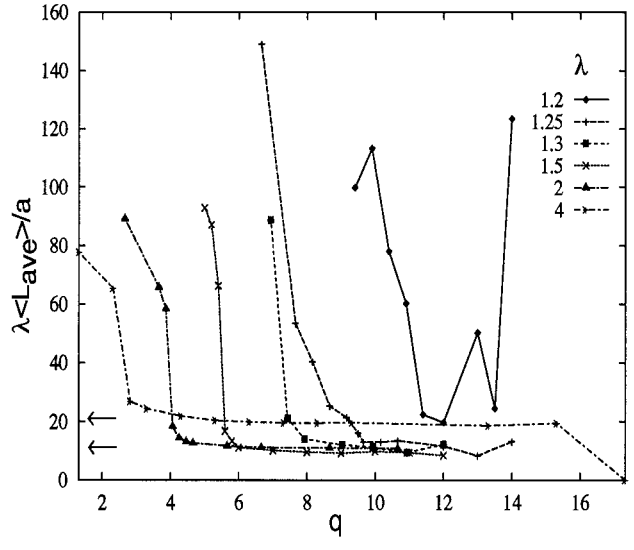

FIGURE 4 Dimensionless average hole perimeter length $\lambda\langle L_{ave}\rangle/a$ as a function of the reduced barrier height q. Data are shown for a 256-vertex network at reduced line tensions $\lambda = 1.2$, 1.25, 1.3, 1.5, 2.0, 4.0. The predictions of the ideal pore gas model in Appendix A, Eq. 12, for the average pore size are marked by arrows for $\lambda = 4$,2 and show good agreement with the simulations. The fluctuations in the data for $\lambda = 1.2$ are discussed in the text.

The line tension λ couples to the total perimeter of all holes, and does not determine the hole size distribution. We find that the total perimeter length of all holes $\langle L_{tot}\rangle/a$, shown in Fig. 5, increases smoothly for all the systems studied. The total hole perimeter length is calculated in each configuration before the ensemble average is performed. When this is compared with $\ln\langle N\rangle$ in Fig. 3, it suggests that the total perimeter length increases as a consequence of a single hole expanding when the line tension is close to λ^*, whereas it is the combined appearance of many small holes that permeabilizes the membrane for large line tensions. This is supported by snapshots of the network configurations. Comparing snapshots *b* and *d* in Fig. 1 shows that a network with $\lambda = 4$ contains many small holes at $q = 4.3$ while still in the regime of constant average hole size, whereas a single hole dominates the network with $\lambda = 1.25$ and $q = 8.2$. Visual examination of the network in the latter case shows that the dominant hole fluctuates greatly. This is illustrated for the case of a 400-vertex network with $\lambda = 1.25$, $q = 8.66$ in Fig. 6, which shows the variation of the average hole perimeter with simulation time. The dynamical nature of the hole is evident, and the ratio of the largest to

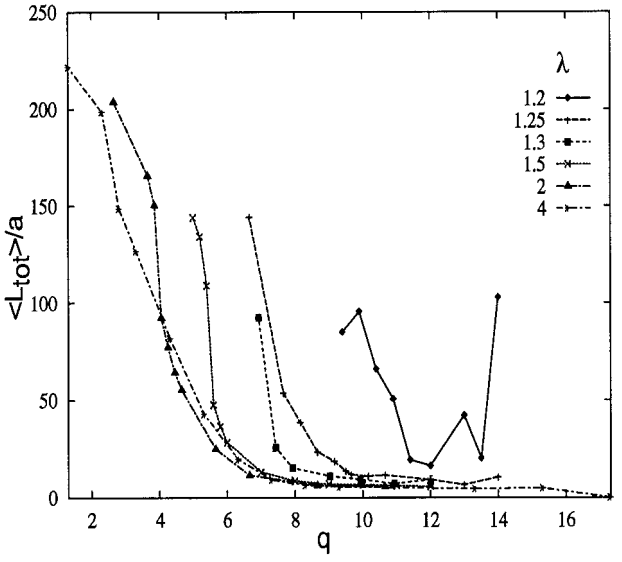

FIGURE 5 Total perimeter length $\langle L_{tot}\rangle/a$ of all holes as a function of the reduced barrier height q. Data are shown for a network of 256 vertices at reduced line tensions $\lambda = 1.2, 1.25, 1.3, 1.5, 2.0, 4.0$. The similarity of the curves for $\lambda \leq 1.5$ to those in Fig. 4 shows that a single hole dominates the rupture process for these line tensions. The fluctuations in the data for $\lambda = 1.2$ are discussed in the text.

smallest (nonzero) hole area is over 600. Examination of individual configurations (not shown) shows that there is only ever a single large hole, although several small holes may appear briefly.

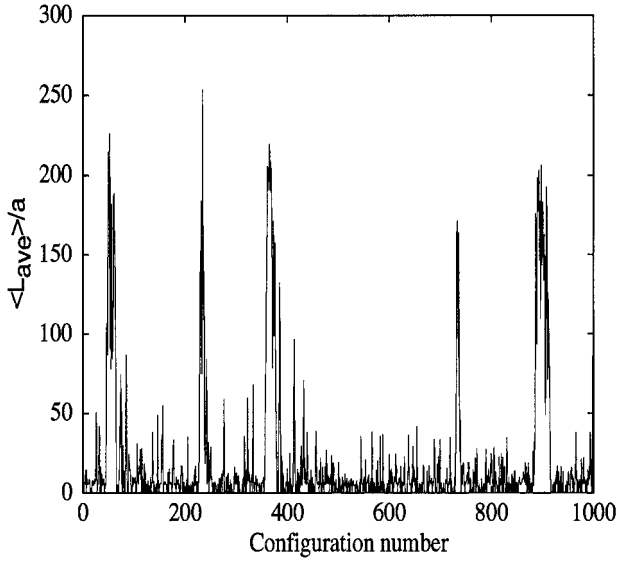

FIGURE 6 Evolution of the average hole perimeter length $\langle L_{ave}\rangle/a$ for a 400-vertex network with $\lambda = 1.25$ and $q = 8.66$ throughout a simulation. Each of the 1000 configurations is separated by 100,000 discarded configurations. The hole size clearly fluctuates greatly, and 318 configurations have no holes at all. The hole perimeter averaged over all configurations is $\langle L_{ave}\rangle/a = 30 \pm 48$, whereas the average number of holes is $\langle N\rangle = 1.44 \pm 0.70$.

Compression modulus

The membrane's reduced area compression modulus $\beta K a^2$ is shown in Fig. 7 as a function of q. It is calculated from the fluctuations in the network area, using the relation $\beta K = \langle A\rangle/(\langle A^2\rangle - \langle A\rangle^2)$ (Shillcock and Boal, 1996). The intact network has a compression modulus $\beta K a^2 \approx 20$ for all of the line tensions studied (Boal et al., 1992; Kantor, 1989). At a line tension $\lambda = 1.25$, the modulus drops sharply from $\beta K a^2 \approx 20$ to zero at a barrier height $q \approx 10$. For larger λ, the modulus remains at the intact network value down to smaller q, but eventually collapses at a nonzero barrier height. Comparing Fig. 7 with Fig. 3 shows that the presence of one or a few fluctuating holes for a line tension $\lambda \gtrsim \lambda^*$ reduces the membrane compression modulus close to zero. However, the small holes created at larger line tensions are essentially immobile because of the energy cost of changing their perimeter, and do not greatly modify the network compression modulus until the membrane enters the unstable regime. For example, a network with $\lambda = 2$ and $q = 5$ has a compression modulus barely altered from the intact value, even though Fig. 3 shows it to have about seven holes. The collapse of the compression modulus is abrupt for all line tensions. However, the fluctuations of the compression modulus (estimated from the standard deviation of the values, calculated by dividing the data from 1000 configurations into 10 groups) are typically 10% for the intact networks, increasing to 30% for the almost vertical portions of the data. For a line tension $\lambda = 1.2$, the intact

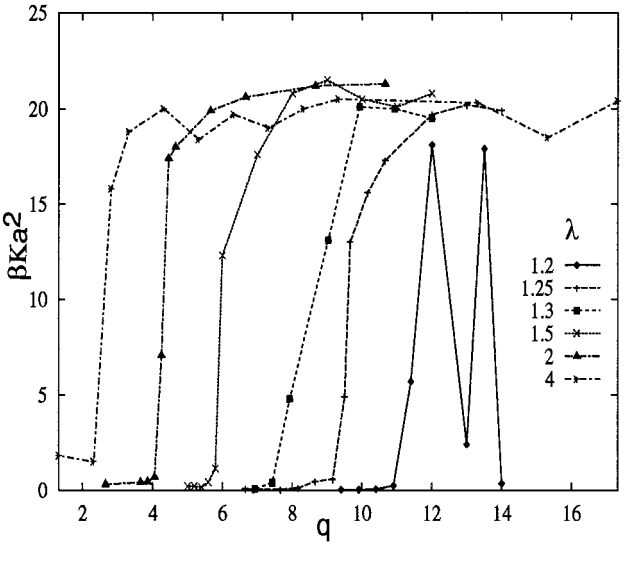

FIGURE 7 Dimensionless fluid network compression modulus $\beta K a^2$ for a 256-vertex network against reduced barrier height q for reduced line tensions $\lambda = 1.2, 1.25, 1.3, 1.5, 2.0, 4.0$. In the absence of holes, the network's compression modulus is that of a pure fluid network, and this value remains approximately unchanged as small holes are created at line tensions $\lambda \geq 1.5$, until the holes start to aggregate. For small line tensions, $\lambda \leq 1.5$, the compression modulus drops precipitously to zero when a fluctuating hole appears in the network. The bimodal nature of the data for $\lambda = 1.2$ results from the lifetime of the intact network approaching the simulation time scale, as discussed in the text.

network state is only metastable, although the simulation time needed for the network to rupture may exceed 10^8 sweeps for $q > 12$. The compression modulus at this line tension appears bimodal as q increases, because it varies between the intact network value (if no hole opens up during a simulation) and zero (if a hole appears). Note that the hole may exist for only a fraction of the simulation time. A hole appeared in the network with $\lambda = 1.2$, $q = 13$ in Fig. 7 for only 2.3% of the simulation time, but the compression modulus fluctuated between $\beta K a^2 = 22$ and 0.8. Inspection of successive configurations of the network showed that a hole appears, fluctuates, and reseals several times, indicating coexistence of the intact network and the ruptured state at this value of line tension. The reduced network compression modulus $\beta K a^2$ depends on the system size in a λ-dependent manner. For $\lambda = 4$, $\beta K a^2$ is independent of N_v for all barrier heights $q > q_R(\lambda)$. The compression modulus of networks with $1.25 \leq \lambda \leq 2$ falls to zero at slightly larger q for larger system sizes. The variation for a network with $\lambda = 1.5$ is $q = 5.4$–5.6 for system sizes $N_v = 144, 196, 256, 400$.

We recall at this point that the model membrane is a fluid, and so its shear modulus is identically zero. All of the computational membranes we discuss have shear moduli that are zero to three decimal places.

Hole size distributions and scaling behavior

Networks with a line tension much greater than λ^* open up more holes as q is reduced, the size of the holes remaining small, until they are forced to aggregate by the finite system size. This is illustrated in Fig. 8, plots *a* and *b*, where the hole perimeter distributions are displayed for $\lambda = 4$ and $q = 9.3, 4.3$. The histograms are normalized so that their total area equals the average hole perimeter length. The network in plot *a* is well into the regime of constant average hole size seen in Fig. 4, where holes are small and infrequent, with 80% of 1000 configurations having no holes at all, whereas that in plot *b* is on the edge of the unstable regime and there are no configurations without holes. The hole perimeter distributions for both networks peak at a minimum hole perimeter and drop rapidly to zero as the perimeter increases. The average hole perimeter is $\langle L_{ave} \rangle / a = 4.89 \pm 0.40$ and $\langle L_{ave} \rangle / a = 5.45 \pm 0.50$ for plots *a* and *b*, respectively. The average number of holes increases from $\langle N \rangle = 1.13 \pm 0.33$ to 15.04 ± 2.60 on reducing the barrier height from $q = 9.3$ to 4.3.

Networks with $\lambda \gtrsim \lambda^*$ show behavior very different from the above. The distribution of hole perimeter lengths for $\lambda = 1.25$ and $q = 10.2, 8.2$ is shown in plots *c* and *d* of Fig. 8. Even at a barrier height $q = 10.2$, when 87% of the 1000 configurations in a simulation have no holes at all, the number of vertices around a hole varies from 4 to ~50. At the lower barrier height, $q = 8.2$, the holes coalesce into a single hole whose perimeter fluctuates greatly, as the distribution in plot *d* shows. The histogram at $q = 8.2$ shows

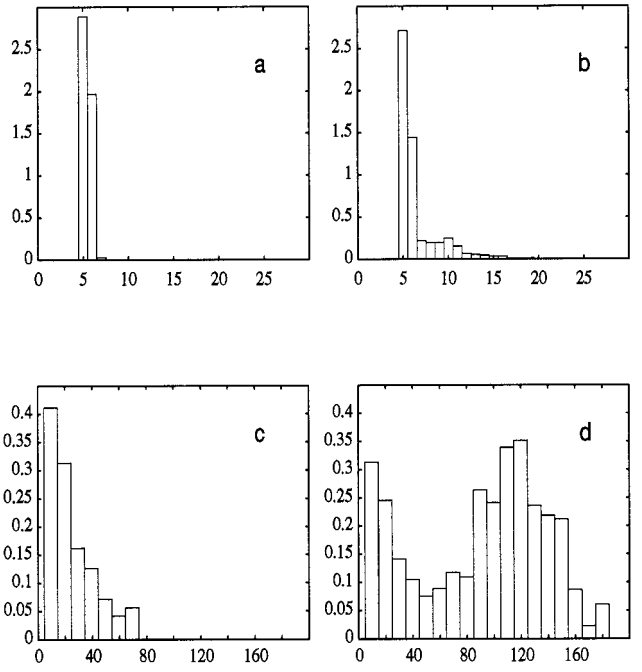

FIGURE 8 Distribution of individual hole perimeters for a network of 256 vertices. The *y* axis is the probability of the hole perimeter length taking a given value multiplied by that value. The histograms are therefore normalized so that their total area equals the average hole perimeter length. The two upper plots show the distribution for a reduced line tension $\lambda = 4$ and reduced barrier heights $q = 9.3$ (*a*) and $q = 4.3$ (*b*), respectively. The holes are predominantly minimal-sized, and the distribution shifts only slightly toward larger holes at smaller q. The two lower plots show the distribution for $\lambda = 1.25$ and $q = 10.2$ (*c*) and $q = 8.2$ (*d*), respectively. The size distribution is broad at both barrier heights, and appears to be bimodal for $q = 8.2$. The bin width in *a* and *b* is $\Delta L/a = 1$, and in *c* and *d* it is $\Delta L/a = 10$. The average hole perimeter lengths for plots *a*–*d* are, respectively, $\langle L_{ave} \rangle / a = 4.89 \pm 0.36, 5.45 \pm 0.49, 11.81 \pm 10.51, 32.28 \pm 40.06$. The average numbers of holes for the plots are given in the text.

a very broad, almost bimodal distribution, with the number of vertices around a hole varying from 4 to over 130, yet with 28% of the configurations still having no holes at all. The average hole perimeter in these cases is $\langle L_{ave} \rangle / a = 11.81 \pm 10.50$ and $\langle L_{ave} \rangle / a = 32.28 \pm 40.10$ for plots *c* and *d*, respectively. That these results are due to a single fluctuating hole, rather than a broad distribution of several holes, is supported by the average hole number changing only from $\langle N \rangle = 1.04 \pm 0.20$ for $q = 10.2$ to 1.40 ± 0.67 for $q = 8.2$. Inspection of the network configurations confirms that there is at most one large hole with one or two occasional small ones in addition.

Like to the perimeter length, the distributions of hole areas at large and small line tensions are qualitatively different. The four plots in Fig. 9 show the hole area distributions corresponding to the networks shown in the previous figure. The areas of holes produced in the network with $\lambda = 4$ are close to zero, and remain so, even near the limit of an unstable membrane. Inspection of the configurations shows that the holes are typically lozenge shaped, as illustrated in plot *b* of Fig. 1. The network with $\lambda = 1.25$ shows much

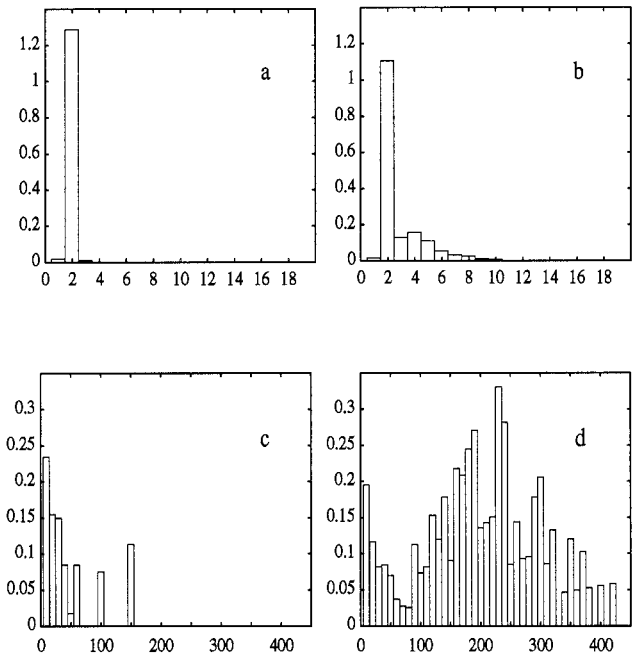

FIGURE 9 Distribution of individual hole areas for a network of 256 vertices. The y axis is the probability of the hole area taking a given value multiplied by that value. The histograms are normalized so that their total area equals the average hole area. The upper two plots show the distributions for $\lambda = 4$ and $q = 9.3$ (a) and $q = 4.3$ (b), respectively. The hole areas are tightly clustered around the average value, shifting only slowly toward larger holes at the lower barrier height. Plots c and d show the distribution for $\lambda = 1.25$ and $q = 10.2$, 8.2, respectively. The hole areas are broadly distributed, showing the absence of a "typical" hole size. The bin width for plots a and b is $\Delta A/a^2 = 1$, whereas that for c and d is $\Delta A/a^2 = 10$. The average hole areas for plots a–d are, respectively, $\langle A_{ave}\rangle/a^2 = 1.32 \pm 0.21$, 1.66 ± 0.29, 9.12 ± 17.20, 49.32 ± 82.76. The average numbers of holes for the plots are given in the text.

larger variation in the hole areas. The distribution in plot c of Fig. 9 has an average area $\langle A_{ave}\rangle/a^2 = 9.12 \pm 17.20$, although there are holes with areas close to $A/a^2 = 150$, and the total hole area $\langle A_{tot}\rangle/a^2 = 9.42 \pm 17.45$ is close to the average area. At the lower barrier height of $q = 8.2$ in plot d, the average hole area is $\langle A_{ave}\rangle/a^2 = 49.32 \pm 82.80$. That the membrane has not disintegrated irreversibly is shown by the repeated disappearance of holes throughout the simulations: there are no holes in the network for 876 and 276 configurations for the distributions in plots c and d of Fig. 9, respectively. The time series of the average hole perimeter in Fig. 6 shows that a large hole appears and reseals repeatedly.

A scaling analysis of the holes present in membranes with between 144 and 400 vertices and $\lambda = 1.25$ shows two distinct behaviours: in the limit of small holes, the area scales with the perimeter like a circle, whereas the area of large holes scales with the perimeter as $A \propto L^{\nu}$, with $\nu = 1.5 \pm 0.1$. The cross-over between the two regimes occurs when $\sim$10–15 vertices are on the hole perimeter. The scaling is independent of the network size N_v. The exponent is extracted by plotting the area of each hole against its perimeter on a log-log plot. Typically more than 2000 holes are used to extract the scaling behavior. Thus the perimeters of holes consisting of more than 10 vertices appear to fluctuate as closed self-avoiding walks. This scaling was previously found in Shillcock and Boal (1996) for a single hole at $\lambda = 1.24$, indicating that the coalescence of holes does not change the scaling behavior of large holes.

It is not possible to perform a scaling analysis on holes in networks with line tensions above $\lambda = 1.5$, as their areas are not widely distributed enough. Because such holes typically have fewer than 10 vertices on their edge, we expect their area to scale with their perimeter as circles.

Influence of multiple holes on tension-induced rupture

When the model membrane is subject to a hydrostatic stretching tension, p, it is metastable against rupture for all values of the line tension. However, the simulation time required for the network to open up a hole may be enormously long. We have performed simulations for networks at various λ and p as a function of q. Because the results for networks under tension will be presented elsewhere (Shillcock, manuscript in preparation), we only comment here on the effects of multiple holes on the approach to rupture.

Our computational definition of a ruptured network under tension differs from that used for tension-free networks. The lateral tension prevents holes from shrinking back to zero once they have reached a certain size. We say that a network is ruptured when the area of the largest hole exceeds one-quarter of the total network area. Such holes were not observed to reseal in the simulations. Whereas small holes may disappear in a network under tension, a large hole is prevented from doing so by the (dominant) contribution of the $-PA_{hole}$ term in its free energy. The MC time required for rupture varies exponentially with q at fixed λ and p (data not shown). This is expected from a simple Kramer's calculation of the rate of thermally activated barrier crossing. However, the appearance of the holes that rupture the network is different for small and large line tensions, as found by examining snapshots of the network state near the computational rupture point. At large λ, an almost circular hole expands in area toward the computational rupture point. In contrast, for line tensions in the range $\lambda = 1.5$–2, the hole in the ruptured network is irregular and fluctuates, even while increasing in area. We conclude that a lateral tension on the network does not completely suppress shape fluctuations of the holes present at small line tensions.

DISCUSSION

The previous models of pore formation in fluid membranes mentioned in the Introduction characterize pores as circular holes. The competition between a lateral tension stretching the membrane and the edge energy of the exposed pore boundary defines a unique radius, below which pores shrink

and reseal and above which their growth is limited only by the size of the membrane. When the entropy of pore shape fluctuations is included in its free energy, a model membrane is unstable to the unrestrained growth of a single hole, even at zero lateral tension and at a critical value of line tension λ^* (Shillcock and Boal, 1996). This forms the boundary to the intact state in Fig. 2 in the limit $q \to \infty$. The curved phase boundary seen in Fig. 2 and parameterized in Eq. 3, and the network snapshots in Fig. 1 indicate that the model membrane's behavior in the λ,q plane is qualitatively different for $\lambda \gg \lambda^*$ and $\lambda \gtrsim \lambda^*$. At large line tensions, the holes are small, increasing in number until the membrane enters the unstable regime. When the line tension is reduced toward $\lambda^*(q)$, a single hole dominates the network, increasingly fluctuating in size and shape until the network ruptures at $\lambda = \lambda^*$. The transition appears to be first order from the bimodal hole size distribution in d of Fig. 8. This bimodality persists even for large line tensions, but it shifts closer to the unstable regime and is difficult to extract reliably (data not shown). Near the rupture transition, the size and shape of the dominant hole fluctuate considerably. We can gain insight into the collective behavior of multiple holes from two extreme models: an ideal gas of circular pores, expected to be applicable in the regime $\lambda \gg \lambda^*$, and a nonlinear growth model in which hole shape fluctuations and coalescence lead to a single large fluctuating hole for $\lambda \to \lambda_R(q) > \lambda^*$.

Lowering q at large λ increases the number of small pores in the computational membrane until they aggregate at $q = q_R(\lambda)$. This corresponds to a physical membrane in which the pores are essentially independent entities whose evolution is governed by the mechanical energy of the pore edge and the external stress creating them. This is the case in electroporation experiments and the models devised to interpret the results (see Freeman et al., 1994, and references therein). The first model described in Appendix A treats the pores as a noninteracting collection of circular holes with an energy proportional to their circumference. The exponential increase in hole number predicted by Eq. 11 is seen in Fig. 3 for networks with line tensions $\lambda \geq 1.5$. Similarly, the dimensionless average hole perimeter $\lambda\langle L_{ave}\rangle/a$ is seen in Fig. 4 to vary with the line tension, as predicted by Eq. 12. The intercepts of the flat portions of the curves agree with the predictions of the ideal pore gas model, as indicated by the arrows in Fig. 4 for $\lambda = 2, 4$.

The typical density of holes of our model system for $\lambda = 4$ and $q = 6.3$ (midway between snapshots a and b in Fig. 1) is $\langle N\rangle/N_v = 0.016$ independent of system size. We can convert this into a physical density as follows. We let room temperature (298 K) set the energy scale, fix the length scale by assuming a typical lipid headgroup diameter of 1 nm, and equate this to the average bond length in the simulations ($\langle L_{bond}/a\rangle = 1.33 \pm 0.20$). The hole density translates into $\sim$4 pores/100 nm^2 in a lipid bilayer membrane with these values. The corresponding density for $q = 4.3$ (snapshot b in Fig. 1) is $\langle N\rangle/N_v = 0.059$, equivalent to 15 pores/100 nm^2.

The critical line tension for rupture of (vesicular) lipid bilayers has been measured to be in the range $1–3 \times 10^{-11}$ N (Zhelev and Needham, 1993). The actual value depends on lipid composition and the addition of cosurfactants (e.g., cholesterol), but appears to be independent of the nature of the stress on the membrane, i.e., an electric field-induced stress and an osmotic stress induce pores equally. We can convert these measurements into a dimensionless line tension λ by relating the simulation parameters to the physical properties of a membrane as above. The experimental line tension range quoted is then $\lambda = 2.4–7.2$. Thus, from the experiments of Zhelev and Needham (1993), one derives a line tension that would keep holes in the computational membrane approximately circular.

The lower line tension derived from the data of Zhelev and Needham (1993) is less than a factor of 2 larger than λ^* in Eq. 4, at which entropy-driven disintegration of the model membrane occurs. The question arises whether there are mechanisms in nature that exploit this closeness of the intact lipid bilayer state to one in which pores are entropically favored. A network with a line tension $\lambda \gtrsim \lambda^*$ has very few holes at large q, and opens up a single hole that increasingly fluctuates through the membrane as q is reduced. That it is the collective behavior of the holes that leads to the dominant hole growth may be understood by considering the second model described in Appendix A. This model assumes that small (hydrophobic) holes created by thermal fluctuations cross a barrier to grow into larger (hydrophilic) holes if the line tension parameter for hydrophilic holes is not too large. The boundary of a large hole fluctuates and grows by absorbing small holes in its immediate vicinity, reducing the density of small holes. The model predicts that at low line tensions and a critical density of small holes, there is a transition from an equilibrium state containing many small holes to a state in which a large hole grows catastrophically. Although it is difficult to make a quantitative comparison with our simulations because of the difficulty of assigning values to the phenomenological constants that appear in the model, the decreasing size of the dominant hole in the computational network with increasing q for line tensions close to λ^* shows that the continual creation of small holes is needed for the hole to grow in this line tension regime.

Recent experiments with the peptide magainin show that lipid bilayers are systematically disrupted by insertion of the peptide into the membrane (Ludtke et al., 1996; Matsuzaki et al., 1997a). It would be interesting to test whether the labile hole boundary found in our simulations for networks with small line tensions is useful in certain biological processes, such as biochemical lysis of bacterial plasma membranes (Matsuzaki et al., 1997a). A first step toward such an understanding would be to systematically investigate the permeabilization of membranes of mixed composition. Zhelev and Needham (1993) have shown that cholesterol increases the line tension of single-component SOPC vesicles, and impurities are known to enhance the leakage of vesicles, but little systematic investigation of pore forma-

tion as a function of vesicle composition is known to the authors.

The dependence of pore formation on multicomponent lipid bilayers could also be simulated. Vertices in the computational network can be "colored" with distinct values for their contribution to the edge energy, corresponding to the varying packing compatibility of different lipids. Spontaneous aggregation of vertices with a low value of edge energy would lead to holes. Simulations extended into three dimensions may provide insight into domain-induced transitions in membranes, such as the budding transition (Lipowsky, 1993), and the effects of edge-active agents in modifying vesicle formation from planer bilayer patches (Fromherz, 1983). Experiments measuring the variation of line tension for lipid bilayers/vesicles of varying composition are a necessary prerequisite for such future work. The increasing awareness of the dynamic nature of lipid bilayers in biological systems suggests that entropy can play an important role in facilitating processes that may at first sight appear to be energetically prohibited. Computer simulations provide an indispensible tool for teasing apart the interactions of energy and entropy.

APPENDIX A

In this appendix we present two simple models that capture the essential features of the hole statistics revealed by the simulations.

Ideal pore gas model

When the line tension around a hole is large enough to suppress shape fluctuations of its perimeter, the behavior of the hole is energy dominated. In the computational membrane, the energy cost of cutting bonds around a hole edge also restricts its lateral motion in the membrane. We can gain insight into the simulation results in this regime by treating the holes as a two-dimensional ideal gas of circular, noninteracting pores. The energy of a pore of radius r_j is proportional to its perimeter, where the proportionality constant Λ is the line tension. We define the model Hamiltonian for a membrane containing N such pores as

$$H = \sum_{j=1}^{N} 2\pi r_j \Lambda. \tag{5}$$

The partition function for the ideal pore gas is

$$Z(T, A, \mu, \Lambda) = \sum_{N=0}^{\infty} e^{\beta\mu N} \sum_{\text{states}} e^{-\beta H}, \tag{6}$$

where T is temperature, A is the area of the membrane, and μ is the chemical potential of the pore gas. The "states" of a pore are labeled by its radius, and because all pores with the same radius are assumed to be identical, we include the usual statistical factor for a gas of indistinguishable particles. The partition function of the pores is therefore that of an ideal Maxwell-Boltzmann gas:

$$Z(T, A, \mu, \Lambda) = \sum_{N=0}^{\infty} e^{\beta\mu N} \sum_{\text{states}} \frac{1}{n_1! n_2! \cdots n_j!} e^{-\beta\lambda\sum_{j=0}^{\infty} 2\pi j n_j}, \tag{7}$$

where there are n_j pores of radius r_j, and we include a minimum pore radius, r_0, to model the expectation that hydrophilic pores are energetically favored only for radii larger than a minimum value (Glaser et al., 1988). The grand potential for such a gas is easily calculated to be

$$\Omega(T, A, \mu, \Lambda) = -k_B T \sum_{j=0}^{\infty} e^{-\beta(2\pi j\Lambda - \mu)}. \tag{8}$$

We now convert the sum over pore states to an integral. This requires the integration measure to be specified. Because a single hole is a two-dimensional object, we define the integration over all possible states of the hole with the measure factor d^2r to account for the increase in the density of states with pore radius. Performing the integral, the grand potential of an ideal gas of circular pores is

$$\beta\Omega(T, A, \mu, \Lambda) = -\frac{1 + 2\pi\beta\Lambda r_0}{(2\pi\beta\Lambda a)^2} e^{-(2\pi\beta\Lambda r_0 - \beta\mu)}. \tag{9}$$

This determines all of the thermodynamic properties of the pore gas. The average total perimeter length of all pores $\langle L\rangle = \partial\Omega/\partial\Lambda$, and the average number of pores $\langle N\rangle = -\partial\Omega/\partial\mu$ are given by

$$\beta\Lambda\langle L\rangle = \frac{(1 + (1 + 2\pi\beta\Lambda r_0)^2)}{(2\pi\beta\Lambda a)^2} e^{-(2\pi\beta\Lambda r_0 - \beta\mu)} \tag{10}$$

$$\langle N\rangle = \frac{1 + 2\pi\beta\Lambda r_0}{(2\pi\beta\Lambda a)^2} e^{-(2\pi\beta\Lambda r_0 - \beta\mu)}. \tag{11}$$

The average pore perimeter is independent of the chemical potential in this model:

$$\frac{\beta\Lambda\langle L\rangle}{\langle N\rangle} = 1 + 2\pi\beta\Lambda r_0 + \frac{1}{1 + 2\pi\beta\Lambda r_0}. \tag{12}$$

We compare this model's predictions with the simulation data by choosing the minimum hole size to be $2\pi r_0/a = 5.33$, as extracted from the simulations, and recalling that $\lambda = \beta\Lambda a$. The average pore perimeter length from Eq. 12 shows good agreement with the numerical data for $\lambda > 2$, as the arrows in Fig. 4 for $\lambda = 4, 2$ show, provided that $q > q_R(\lambda)$. Within the ideal pore gas model, there is no rupture transition for $\lambda > 0$; only as λ approaches zero do the thermodynamic quantities diverge.

Nonlinear dynamical model of pore interactions

The opposite extreme of the ideal pore gas model is to consider pores that fluctuate in shape, translate freely, and aggregate or split up. Such a model may be constructed by using the nonlinear growth equations taken from chemical reaction models (Reichl, 1980). Consider a model membrane composed of lipid molecules that may be in one of three states: in the bulk L_α fluid state; on the edge of a hydrophobic (HO) pore; and rotated onto the edge of a hydrophilic (HI) pore. Let $N_1(t)$, $N_2(t)$ be the total number of lipids on the edge of HO and HI pores, respectively, at time t.

Thermal fluctuations continually create small, transient HO pores as the lipid headgroups move apart. The effect of a stressor, such as an electric field, has been interpreted as lowering the energy barrier against such HO pores. The number of lipids around the edge of HO pores increases as more pores are created, and we characterize this process by a rate constant c. Spontaneous resealing of pores reduces the number of lipids around HO pores and is represented by the term $-dN_1(t)$, where d gives the fraction of HO pores that reseal per unit time. If an HO pore grows large enough that the hydrophobic energy cost of the exposed lipid hydrocarbon chains exceeds that of rearranging the lipids, so that their headgroups point into the pore channel, the HO pore changes into an HI pore. The minimum radius at which it becomes favorable for HO pores to rearrange into HI pores has been estimated to be ~1 nm (Glaser et al., 1988). We consider all HO pores to have the same small radius and represent the probability of

their transforming into HI pores by a rate constant x. The inverse process of an HI pore converting back to an HO pore is represented by a rate constant y. We assume that HI pores can only be created as a result of HO pores crossing an energy barrier, so that these parameters satisfy the inequality $x \leq y$.

We next assume that HI pores grow as the result of fluctuations of their boundaries absorbing HO pores in their vicinity, and represent this process by a nonlinear term that increases the number of lipids on the edge of HI pores by reducing the HO pore density. We add a term to the growth equations that depends on the probability of an HO and HI pore intersecting, N_1N_2, with a coefficient of proportionality r. If $r \simeq 0$, the pores are essentially independent, whereas a large value of r allows HI pores to grow by absorbing HO pores. We focus on this process rather than on HI pores simply growing into the surrounding bulk membrane for two reasons. The simulations show that increasing the barrier height against hole creation for small line tensions drastically reduces the size of the dominant hole, suggesting that hole growth in this regime of line tension is driven by the creation rate of small holes, and allowing HI pores to grow into the bulk membrane only increases the probability that neighboring HO pores will be absorbed by the growing HI pores.

Combining these processes into growth equations for the numbers of lipids around HO and HI pores gives (a dot indicates a time derivative)

$$\begin{aligned} \dot{N}_1(t) &= c - (d + x)N_1 + yN_2 - rN_1N_2 \\ \dot{N}_2(t) &= xN_1 - yN_2 + rN_1N_2. \end{aligned} \tag{13}$$

Clearly, other processes could be included in this scheme, such as HO pores combining to form HI pores, or other nonlinear dependences of the densities, but the above scheme already contains interesting results.

We solve Eq. 13 for the linearized steady state ($r = 0$) to get

$$\bar{N}_1 = \frac{c}{d}, \quad \bar{N}_2 = \frac{x}{y}\bar{N}_1. \tag{14}$$

Because the ratio x/y satisfies the inequalities $0 < x/y \leq 1$, the number of HI pores is less than the number of HO pores in the linearized steady state, and the membrane is stable against HI pores growing. However, this solution may be unstable as the parameter r is increased because of the presence of the nonlinear term, and a new steady-state solution may appear. The nonlinear steady-state solution is

$$\bar{N}_1 = \frac{c}{d}, \quad \bar{N}_2 = \frac{xcd}{yd^2 - cdr} = \frac{x\bar{N}_1}{y - r\bar{N}_1}. \tag{15}$$

The linearized steady-state solution becomes unstable as the quantities r and c/d are varied when the denominator in the second equation vanishes. A linear stability analysis of Eq. 13 shows that the behavior of the solutions is controlled by the eigenvalues of the stability matrix $\lambda_\pm = -\omega \pm \sqrt{\omega^2 - d(y - rN_1)}$, where $\omega = 1/2(d + x + y + r(\bar{N}_2 - \bar{N}_1))$. The linear solution is stable when the real parts of both eigenvalues are negative. This is violated when $\bar{N}_1 > y/r$, a condition relating the mean number of HO pores to the probability of an HI pore absorbing an HO pore. We relate Eq. 15 to the simulation results by noting that a large line tension reduces the probability of HO pores growing into HI pores ($x/y \ll 1$), and keeps HI pores small, thereby reducing their interactions ($r \approx 0$). Increasing the HO pore creation rate increases their number, but there are few HI pores. The linearized steady state is therefore stable at large line tensions. At small line tensions, the probability of HO pores converting into HI pores is higher ($x/y \approx 1$), and the HI pore shape fluctuations increase the probability of absorption of nearby HO pores ($r > 0$). Increasing the HO pore density causes the newly created pores to be absorbed by the fluctuating HI pores, and the linearized steady state becomes unstable to a new state, in which the number of lipids on the boundary of HI pores increases catastrophically. Notice that the model does not distinguish between the case of a single HI pore or many such pores with the same total perimeter length. But it is clear that the nonlinear interaction term is essential for the appearance of a large HI pore.

APPENDIX B: HOLE GROWTH AND NETWORK FLUIDITY ALGORITHMS

Here we describe the algorithms used to simulate the appearance, growth, and interactions of holes in the computational network.

We apply the Metropolis algorithm to evolve the state of the network. A sweep across the network consists of the following attempted moves: 1) Each vertex is translated by random amounts selected from a square box of size $2\Delta s$ centered on the vertex's current position, and the move is accepted with the usual Boltzmann factor. The step size Δs is close to $0.2a$ so as to keep the average acceptance rate for translational moves around one-half. 2) The bond removal/add moves described below are applied to N_v randomly selected vertices. 3) An attempt is made to flip all internal bonds to their adjacent vertices. 4) An attempt is made to rescale the simulation box area by adding to the box lengths L_x, L_y independent random amounts selected on the interval $(-\Delta L, +\Delta L)$ (see Hansen and McDonald, 1986, for details), simultaneously rescaling all vertex coordinates by the same amount. The rescaling is accepted if no pair of vertices overlaps and no bond exceeds its maximum length. The area rescaling step size ΔL is typically $0.01a$. If any move fails, the old network configuration is counted as the new state. In the limit of an infinite chain of moves, the probability of occurrence of a configuration approaches its Boltzmann weight.

The following steps are used to implement move 2) above. A vertex is randomly chosen from the N_v in the network, and an attempt is made, with probability one-half, to remove a bond connected to it; otherwise an attempt is made to add a bond back. A hole is created if the selected vertex is internal, by removing one of its attached bonds selected at random if a random number uniformly selected on the interval (0, 1) is less than the Boltzmann factor $\exp(-q)$. The barrier height against hole creation is $q = \beta(\Lambda L_{min} - \mu)$, where L_{min} is the dynamically calculated summed length of the newly external bonds, and q is a "chemical potential" parameter used to provide a connection with the ideal pore gas model. The minimum hole perimeter is always close to $L_{min}/a = 5.33$, and this relates the barrier height q to the chemical potential q. An attempt to add a bond to an internal vertex fails, and in this case the old network state is counted again.

If an external vertex is selected, bonds are removed from the hole boundary or added back, as described in Shillcock and Boal (1996). Because the line tension is positive, attempts to shrink the boundary of a hole always succeed if the new bond satisfies the length restrictions and does not intersect another bond. A hole reseals when it has only four vertices on its boundary and a bond is successfully added across it. Detailed balance is satisfied by adding a bond to a vertex with the same probability with which it would be removed. If the removal of an external bond would result in a vertex being on the boundaries of two holes, then an attempt is made to allow the holes to coalsesce. Conversely, if two vertices around a single hole approach within a distance that would allow a bond to be added between them, then the hole may fragment into two smaller ones. The probabilities of coalescence and fragmentation satisfy detailed balance.

JCS gratefully acknowledges financial support from the Max Planck Gesellschaft.

REFERENCES

Abidor, I. G., V. B. Arakelyan, L. V. Chernomordik, Yu. A. Chizmadzhev, V. F. Pastushenko, and M. R. Tarasevich. 1979. Electric breakdown of bilayer lipid membranes. 1. The main experimental facts and their qualitative discussion. *Bioelectrochem. Bioenerg.* 6:37–52.

Barnett, A., and J. C. Weaver. 1991. Electroporation: a unified, quantitative theory of reversible electrical breakdown and mechanical rupture in artificial planar bilayer membranes. *Bioelectrochem. Bioenerg.* 25: 163–182.

Baumgartner, A., and J-S. Ho. 1990. Crumpling of fluid vesicles. *Phys. Rev. A.* 41:5747–5750.

Beschiaschvili, G., and J. Seelig. 1991. Peptide binding to lipid membranes. Spectroscopic studies on the insertion of a cyclic somatostatin analog into phospholipid bilayers. *Biochim. Biophys. Acta.* 1061:78–84.

Boal, D. H., and M. Rao. 1992. Topology changes in fluid membranes. *Phys. Rev. A.* 46:3037–3045.

Boal, D. H., U. Seifert, and A. Zilker. 1992. Dual network model for red blood cell membranes. *Phys. Rev. Lett.* 69:3405–3408.

Crowley, J. M. 1973. Electrical breakdown of bimolecular lipid membranes as an electromechanical instability. *Biophys. J.* 13:711–724.

Dimitrova, M. N., and H. Matsumura. 1997. Protein-induced leakage and membrane destabilization of phosphatidylcholine and phosphatidylserine liposomes. *Colloids Surf. B Biointerfaces.* 8:287–294.

Freeman, S. A., M. A. Wang, and J. C. Weaver. 1994. Theory of electroporation of planar bilayer membranes: predictions of the aqueous area, change in capacitance, and pore-pore separation. *Biophys. J.* 67:42–56.

Fromherz, P. 1983. Lipid-vesicle structure: size control by edge-active agents. *Chem. Phys. Lett.* 94:259–266.

Ghosh, A. K., N. Pore, R. Basu, S. De, and P. Nandy. 1996. Lipid perturbation by corticosteroids: an anisotropic study. *Colloids Surf. B Biointerfaces.* 7:65–68.

Glaser, R. W., S. L. Leikin, L. V. Chernomordik, V. F. Pastushenko, and A. I. Sokirko. 1988. Reversible electrical breakdown of lipid bilayers: formation and evolution of pores. *Biochim. Biophys. Acta.* 940:275–287.

Hallett, F. R., J. Marsh, B. G. Nickel, and J. M. Wood. 1993. Mechanical properties of vesicles. *Biophys. J.* 64:426–434.

Hansen, J. P., and I. R. Macdonald. 1986. Theory of Simple Liquids, 2nd Ed. Academic Press, London.

He, K., S. J. Ludtke, D. I. Worcester, and H. W. Huang. 1996. Neutron scattering in the plane of membrane: structure of alamethicin pores. *Biophys. J.* 70:2659–2666.

Helfrich, W. 1974. The size of bilayer vesicles generated by sonification. *Phys. Lett.* 50A:115–116.

Heller, W. T., K. He, S. J. Ludtke, T. A. Harroun, and H. W. Huang. 1997. Effect of changing the size of lipid headgroup on peptide insertion into membranes. *Biophys. J.* 73:239–244.

Hibino, M., H. Itoh, and K. Kinosita, Jr. 1993. Time course of cell electroporation as revealed by submicrosecond imaging of transmembrane potential. *Biophys. J.* 64:1789–1800.

Huang, H. W, and Y. Wu. 1991. Lipid-alamethicin interactions influence alamethicin orientation. *Biophys. J.* 60:1079–1087.

Kantor, Y. 1989. Entropic elasticity of tethered solids. *Phys. Rev. A.* 39:6582–6586.

Kantor, Y., M. Kardar, and D. R. Nelson. 1986. Statistical mechanics of tethered surfaces. *Phys. Rev. Lett.* 57:791–794.

Kashchiev, D., and D. Exerowa. 1983. Bilayer lipid membrane permeation and rupture due to hole formation. *Biochim. Biophys. Acta.* 732: 133–145.

Komatsu, H., and S. Okada. 1996. Ethanol-enhanced permeation of phosphatidylcholine/phosphatidylethanolamine mixed liposomal membranes due to ethanol-induced lateral phase separation. *Biochim. Biophys. Acta.* 1283:73–79.

Ladokhin, A. S., M. E. Selsted, and S. H. White. 1997. Bilayer interactions of indolicidin, a small antimicrobial peptide rich in tryptophan, proline and basic amino acids. *Biophys. J.* 72:794–805.

Lipowsky, R. 1993. Domain-induced budding of fluid membranes. *Biophys. J.* 64:1133–1138.

Litster, J. D. 1975. Stability of lipid bilayers and red blood cell membranes. *Phys. Lett.* 53A:193–194.

Ludtke, S. J., K. He, W. T. Heller, T. A. Harroun, L. Yang, and H. W. Huang. 1996. Membrane pores induced by magainin. *Biochemistry.* 35:13723–13728.

Matsuzaki, K., K. Sugishita, M. Harada, N. Fujii, and K. Miyajima. 1997a. Interactions of antimicrobial peptide, magainin 2, with outer and inner membranes of gram-negative bacteria. *Biochim. Biophys. Acta.* 1327: 119–130.

Matsuzaki, K., S. Yoneyama, and K. Miyajima. 1997b. Pore formation and translocation of melittin. *Biophys. J.* 73:831–838.

Moroz, J. D., and P. Nelson. 1997. Dynamically stabilised pores in bilayer membranes. *Biophys. J.* 72:2211–2216.

Müller, M., and M. Schick. 1996. Structure and nucleation of pores in polymeric bilayers: a Monte Carlo simulation. *J. Chem. Phys.* 105: 8282–8292.

Needham, D., and R. M. Hochmuth. 1989. Electro-mechanical permeabilization of lipid vesicles. *Biophys. J.* 55:1001–1009.

Netz, R., and M. Schick. 1996. Pore formation and rupture in fluid bilayers. *Phys. Rev. E.* 53:3875–3885.

Neumann, E., and S. Kakorin. 1996. Electrooptics of membrane electroporation and vesicle shape deformation. *Curr. Opin. Colloid Interface Sci.* 1:790–799.

Parasassi, T., A. M. Giusti, M. Raimondi, and E. Gratton. 1995. Abrupt modifications of phospholipid bilayer properties at critical cholesterol concentrations. *Biophys. J.* 68:1895–1902.

Popescu, D., C. Rucareanu, and Gh. Victor. 1991. A model for the appearance of statistical pores in membranes due to self-oscillations. *Bioelectrochem. Bioenerg.* 25:91–103.

Reichl, L. 1980. A Modern Course in Statistical Physics. University of Texas Press, Austin, TX.

Sabra, M. C., K. Jorgensen, and O. G. Mouritsen. 1996. Lindane suppresses the lipid-bilayer permeability in the main transition region. *Biochim. Biophys. Acta.* 1282:85–92.

Sackmann, E., 1995. Biological membranes: architecture and function. *In* Structure and Dynamics of Membranes. R. Lipowsky and E. Sackmann, editors. Elsevier/North-Holland, Amsterdam. 1–63.

Shibata, A., K. Ikawa, T. Shimooka, and H. Terada. 1994. Significant stabilization of the phosphatidylcholine bilayer structure by incorporation of small amounts of cardiolipin. *Biochim. Biophys. Acta.* 1192: 71–78.

Shillcock, J. C. 1995. Elastic properties of polymerised and fluid membranes under stress. Ph.D. thesis. Simon Fraser University, Vancouver, BC, Canada.

Shillcock, J. C., and D. H. Boal. 1996. Entropy-driven instability and rupture of fluid membranes. *Biophys. J.* 71:317–326.

Sugar, I. P., and E. Neumann. 1984. Stochastic model for electric field-induced membrane pores electroporation. *Biophys. Chem.* 19:211–225.

Tanford, C. 1991. The Hydrophobic Effect: Formation of Micelles and Biological Membranes, 2nd Ed. Krieger Publishing Company, Melboourne, FL.

Taupin, C., M. Dvolaitzky, and C. Sauterey. 1975. Osmotic pressure induced pores in phospholipid vesicles. *Biochemistry.* 14:4771–4775.

Wilhelm, C., M. Winterhalter, U. Zimmermann, and R. Benz. 1993. Kinetics of pore size during irreversible electrical breakdown of lipid bilayer membranes. *Biophys. J.* 64:121–128.

Winterhalter, M. 1996. Liposomes in electric fields. *In* Handbook of Nonmedical Applications of Liposomes. D. D. Lasic and Y. Barenholz, editors. CRC Press, Boca Raton, FL. 285–307.

Wu, Y., K. He, S. J. Ludtke, and H. W. Huang. 1995. X-ray diffraction study of lipid bilayer membranes interacting with amphiphilic helical peptides: diphytanoylphosphatidylcholine with alamethicin at low concentrations. *Biophys. J.* 68:2361–2369.

Zhelev, D. V., and D. Needham. 1993. Tension-stabilised pores in giant vesicles: determination of pore size and line tension. *Biochim. Biophys. Acta.* 1147:89–104.